Weakened aerosol-radiation interaction exacerbating ozone pollution in eastern China since China's clean air actions

Hao Yang[1,2], Lei Chen[1], Hong Liao[1], Jia Zhu[1], Wenjie Wang[3], Xin Li[3]

[1]Jiangsu Key Laboratory of Atmospheric Environment Monitoring and Pollution Control, Jiangsu Collaborative Innovation Center of Atmospheric Environment and Equipment Technology, School of Environmental Science and Engineering, Nanjing University of Information Science & Technology, Nanjing 210044, China

[2]College of Materials Science and Engineering, Guizhou Minzu University, Guiyang 550025, China

[3]State Joint Key Laboratory of Environmental Simulation and Pollution Control, College of Environmental Sciences and Engineering, Peking University, Beijing 100871, China

Correspondence to: Lei Chen (chenlei@nuist.edu.cn) and Hong Liao (hongliao@nuist.edu.cn)

Abstract

Since China's clean air action, $PM_{2.5}$ air quality has been improved while ozone (O_3) pollution has been becoming severe. Here we apply a coupled meteorology-chemistry model (WRF-Chem) to quantify the responses of aerosol-radiation interaction (ARI), including aerosol-photolysis interaction (API) related to photolysis rate change and aerosol-radiation feedback (ARF) related to meteorological fields change, to anthropogenic emission reductions from 2013 to 2017, and their contributions to O_3 increases over eastern China in summer and winter. Sensitivity experiments show that the decreased anthropogenic emissions play a more prominent role for the increased MDA8 O_3 both in summer (+1.96 ppb vs. +0.07 ppb) and winter (+3.56 ppb vs. -1.08 ppb) than the impacts of changed meteorological conditions in urban areas. The decreased $PM_{2.5}$ caused by emission reduction can result in a weaker impact of ARI on O_3 concentrations, which poses a superimposed effect on the worsened O_3 air quality. The weakened ARI due to decreased anthropogenic emission aggravates the summer (winter) O_3 pollution by +0.81 ppb (+0.63 ppb) averaged over eastern China, with weakened API and ARF contributing 55.6% (61.9%) and 44.4% (38.1%), respectively. This superimposed effect is more significant for urban areas during summer (+1.77 ppb). Process analysis indicates that the enhanced chemical production is the dominant process for the increased O_3 concentrations caused by weakened ARI both in summer and winter. This study innovatively reveals the adverse effect of weakened aerosol-radiation interaction due to decreased anthropogenic emissions on O_3 air quality, indicating more stringent coordinated air pollution control strategies should be made for significant improvements in future air quality.

1. Introduction

With the implementation of clean air action since 2013, $PM_{2.5}$ (particulate matter with an aerodynamic equivalent diameter of 2.5 micrometers or less) concentrations have decreased significantly in China (Zhai et al., 2019; Zhang et al., 2019). However, ozone (O_3) pollution is becoming worse and poses a significant challenge over eastern China, especially in the developed city clusters including Beijing-Tianjin-Hebei (BTH), Yangtze River Delta (YRD), Pearl River Delta (PRD), and Sichuan Basin (SCB) (Lu et al., 2018; Dang and Liao, 2019; Li et al., 2019; Li et al., 2021). According to observation data, Li et al. (2020) found that the daily maximum 8-h average O_3 concentrations (MDA8 O_3) increased at a rate of 1.9 ppb a^{-1} from 2013 to 2019 over eastern China. Elevated O_3 concentrations can not only decrease crop yield but also damage human health (Lelieveld et al., 2015; Yue et al., 2017; Mills et al., 2018). Therefore, it is essential to gain a comprehensive understanding about factors driving the increasing trend of O_3 in China in order to formulate effective prevention strategies.

As a secondary air pollutant, troposphere O_3 can be produced by nitrogen oxides (NO_x = NO + NO_2), carbon monoxide (CO), methane (CH_4) and volatile organic compounds (VOCs) in the presence of solar radiation through photochemical reactions (Atkinson, 2000; Seinfeld and Pandis, 2006). The concentration of O_3 in the troposphere is influenced by changes in meteorological conditions (e.g., high temperature and low relative humidity) and its precursors emissions (e.g., NOx and VOCs) (Wang et al., 2019; Liu and Wang, 2020a,b; Shu et al., 2020). Most precursors are from anthropogenic sources, and some precursors can come from natural sources, such as biogenic VOCs and soil and lightning NOx. Moreover, particulates can also affect O_3 concentrations through aerosol-radiation interaction (ARI), including aerosol-photolysis interaction (API) and aerosol-radiation feedback (ARF) (Liao et al., 1999; Wang et al., 2016; Zhu et al., 2021; Yang et al., 2022), and heterogeneous chemistry on aerosol surface (Lou et al., 2014; Li et al., 2019; Liu and Wang, 2020b). Many studies have found that the decreased $PM_{2.5}$ can be one of the driving factors contributing to the increased O_3 concentrations (Li et al., 2019; Liu and Wang, 2020b;

Shao et al., 2021). Li et al. (2019) analyzed GEOS-Chem simulation results and pointed out that the reductions in $PM_{2.5}$ concentrations from 2013 to 2017 in North China Plain (NCP) could decrease the sink of HO_2 on aerosol surface, which would result in the increase in O_3 concentrations. When heterogeneous reactions were considered in WRF-CMAQ, Liu and Wang (2020b) found that decreased $PM_{2.5}$ concentrations weakened the uptake of reactive gases (mainly HO_2 and O_3) which led to the increase in O_3 concentrations over China from 2013 to 2017. However, the contribution of weakened aerosol-radiation interaction due to substantial decreases in $PM_{2.5}$ under clean air action to the increased O_3 has not been systematically quantified. Furthermore, previous studies mainly focus on the increased summer O_3 (Li et al., 2019; Liu and Wang, 2020a,b; Shu et al., 2020; Shao et al., 2021), but underlying reasons driven the changes in winter O_3 is unclear. Li et al. (2021) pointed out that O_3 pollution has been extended into cold seasons under the emission control measures. Therefore, this study aims to quantify the response of aerosol-radiation interaction to anthropogenic emission reduction from 2013 to 2017, with the mainly focus on the contribution to changed O_3 concentrations over eastern China both in summer and winter.

Aerosol-radiation interaction (ARI) can alter photolysis rates through aerosol-photolysis interaction (API) and meteorological variables through aerosol-radiation feedback (ARF) to influence the formation of O_3 (Yang et al., 2022). API can affect O_3 directly by reducing the photochemical reactions, which weaken the chemical contribution and reduce the surface O_3 concentrations. ARF indirectly affects O_3 concentrations by altering meteorological variables, e.g. by reducing the height of the planetary boundary layer. The suppressed planetary boundary layer can weaken the vertical mixing of O_3 by turbulence and affect the concentration of O_3 precursors. Hong et al. (2020) used WRF-CMAQ in conjunction with future emission scenarios to find that weakened ARF due to reduced aerosol concentration has either negative or positive impacts on the daily maximum 1-h average O_3 concentration in eastern China from 2010 to 2050 due to the changed precursor level caused by the weakened ARF. By using WRF-CMAQ, Liu and Wang (2020b) reported that weakened API could increase the MDA8 O_3 concentrations by 0.3 ppb in urban areas from 2013 to 2017. Zhu et al.

(2021) used WRF-Chem to investigate the impact of weakened ARF on air pollutants over NCP during COVID-19 lockdown and reported that the weakened ARF would increase the O_3 concentrations by 7.8% due to the increased northwesterly and planetary boundary layer height caused by the weakened ARF. In general, previous studies mainly examined the impact of either weakened ARF or API, systematic analysis about the total and the respective impacts of changed API and/or ARF on O_3 over eastern China both in summer and winter from 2013 to 2017 have not been conducted.

The objective of this manuscript is to examine the impacts of aerosol-radiation interactions (ARI), including the effects of aerosol-photolysis interaction (API) and aerosol-radiation feedback (ARF), on O_3 concentrations over eastern China both in summer and winter by using the online coupled WRF-Chem model, with the main focus on their responses to clean air action. Process analysis is also applied to explore the prominent physical/chemical process responsible for the changed impacts of API and/or ARF on surface O_3. This study is believed to provide insights into the role of weakened ARI on O_3 levels over eastern China not only in summer, but also in winter. In Section 2, we describe the model configuration, numerical experiments, observational data, and the integrated process rate analysis. Model evaluation is presented in Section 3. Results and discussions are presented in Section 4. Conclusions are provided in Section 5.

2. Methodology

2.1 Model configuration

The model used in this study is an online-coupled meteorology-chemistry model, Weather Research and Forecasting with Chemistry model (WRF-Chem v3.7.1), that can simulate meteorological fields and concentrations of gases and aerosols simultaneously (Grell et al., 2005; Skamarock et al., 2008). Figure S1 shows the simulated domain that covers most regions of China with a horizontal resolution of 27 km and grid points of 167 (west–east) × 167 (south–north). The model contains 32 vertical levels extending from the surface to 50 hPa, with the first 16 layers located below 2 km to resolve fine boundary layer processes. The enclosed black line in Figure S1 represents the eastern China (22-41.5 °N, 102-123 °E), and the four heavily polluted

regions are also selected for analysis, including BTH (36.0-41.5 °N, 113-119.5 °E), YRD (29.5-32.5 °N, 118-122 °E), PRD (21-23.5 °N, 112-116 °E), and SCB (27.5-31.5 °N, 102.5-107.5 °E), respectively.

The National Center for Environmental Prediction (NCEP) Final Analysis dataset (FNL) with a spatial resolution of 1° × 1° and 6-hour temporal resolution are used to provide the meteorological initial and lateral boundary conditions. The chemical initial and boundary conditions for the WRF-Chem model are taken from the outputs of Community Atmosphere Model with Chemistry (CAM-Chem).

The Carbon Bond Mechanism Z (CBM-Z) is applied as the gas-phase chemical mechanism (Zaveri and Peters, 1999), and the full 8-bin MOSAIC (Model for Simulating Aerosol Interactions and Chemistry) aerosol module with aqueous chemistry is used to simulate aerosol evolution (Zaveri et al., 2008). In MOSAIC module, aerosols are assumed to be internally mixed into 8 bins (0.039–0.078 μm, 0.078–0.156 μm, 0.156–0.312 μm, 0.312–0.625 μm, 0.625–1.25 μm, 1.25–2.5 μm, 2.5–5.0 μm and 5.0–10 μm), and each bin considers all major aerosol species, such as sulfate (SO_4^{2-}), nitrate (NO_3^-), ammonium (NH_4^+), black carbon (BC), organic carbon (OC), and other inorganic mass. The impacts of aerosols on photolysis rates are calculated by using the Fast-J scheme (Wild et al., 2000). The following physical parameterizations are used in WRF-Chem. The Rapid Radiative Transfer Model for general circulation models (RRTMG) scheme is used to treat both shortwave and longwave radiation in the atmosphere (Iacono et al., 2008). The Purdue Lin microphysics scheme (Lin et al., 1983) and the Grell 3D ensemble scheme (Grell, 1993) are used to describe the cloud microphysical and cumulus convective processes. The Noah land surface scheme (Chen and Dudhia, 2001) and the Monin-Obukhov surface scheme (Foken, 2006) are used to simulate land-atmosphere interactions. The planetary boundary layer is characterized by Yonsei University PBL scheme (Hong et al 2006). The main physical and chemical schemes used in this study are summarised in Table S1.

In this study, Multi-resolution Emission Inventory for China (MEIC; http://www.meicmodel.org/) in 2013 and 2017 are used as the anthropogenic emissions of particles and gases (Zheng et al., 2018). Biogenic emissions are calculated online by

using the Model of Emissions of Gases and Aerosols from Nature (MEGAN) developed by Guenther et al. (2006).

2.2 Numerical experiments

Seven sensitivity experiments are designed (Table 1). Here are the detailed descriptions:

(1) BASE_17E17M: This baseline experiment is coupled with the interactions between aerosol and radiation, which includes the impacts of API and ARF. Both the meteorological field and anthropogenic emission are from the year of 2017.

(2) BASE_13E13M: Same as BASE_17E17M, but the meteorological field and anthropogenic emission are from the year of 2013.

(3) NOAPI_17E17M: Same as BASE_17E17M, but the impact of API is not considered by turning off the aerosol effect in the photolysis module, following the method described in Yang et al. (2022).

(4) NOALL_17E17M: Same as BASE_17E17M, but neither the impact of API nor ARF is considered by zeroing the aerosol optical properties in the optical module, following the method described in Yang et al. (2022).

(5) BASE_13E17M: Same as BASE_17E17M, but the anthropogenic emission is from the year of 2013.

(6) NOAPI_13E17M: Same as NOAPI_17E17M, but the anthropogenic emission is from the year of 2013.

(7) NOALL_13E17M: Same as NOALL_17E17M, but the anthropogenic emission is from the year of 2013.

Figure 1 detailedly presents the schematic overview of designed numerical experiments. As shown in Fig. 1, the differences between BASE_17E17M and BASE_13E13M (BASE_17E17M minus BASE_13E13M) represent the changed O_3 (ΔO_3) due to variations in meteorology and anthropogenic emissions from 2013 to 2017. The differences between BASE_13E17M and BASE_13E13M (BASE_13E17M minus BASE_13E13M) show the impact of changed meteorological conditions on O_3 (ΔO_3_MET) from 2013 to 2017. The differences between BASE_17E17M and

BASE_13E17M (BASE_17E17M minus BASE_13E17M) indicate the impact of anthropogenic emission reductions on O_3 (ΔO_3_EMI) from 2013 to 2017.

The impacts of aerosol-radiation interaction (ARI) on O_3 under different anthropogenic emission scenarios (i.e., strong anthropogenic emission levels in year 2013, and weaker anthropogenic emission levels in year 2017) can be analyzed as the differences between BASE_17E17M and NOALL_17E17M (BASE_17E17M minus NOALL_17E17M, denote as ΔO_3_ARI_{17E}), and BASE_13E17M and NOALL_13E17M (BASE_13E17M minus NOALL_13E17M, denote as ΔO_3_ARI_{13E}). The ΔO_3_ARI_{17E} means that the impact of ARI on O_3 at the condition of both the meteorological field and anthropogenic emission are from the year of 2017, and the ΔO_3_ARI_{13E} means that the effect of ARI on O_3 at the state of meteorological field used in the year 2017 and anthropogenic emission applied in the year 2013. In order to quantify the impacts caused by the decreased anthropogenic emission from 2013 to 2017, the impacts of changed meteorological variables should be removed by fixing the meteorological fields in year 2017 in sensitivity experiments. Thus, the impact of weakened ARI due to decreased anthropogenic emission from 2013 to 2017 on O_3 (denote as ΔO_3_ΔARI_EMI) can be quantified from the differences between ΔO_3_ARI_{17E} and ΔO_3_ARI_{13E}. Similarly, the impacts of weakened API (denote as ΔO_3_ΔAPI_EMI) and ARF (denote as ΔO_3_ΔARF_EMI) due to decreased anthropogenic emission on O_3 can also be estimated from the differences between (BASE_17E17M minus NOAPI_17E17M, denote as ΔO_3_API_{17E}) and (BASE_13E17M minus NOAPI_13E17M, denote as ΔO_3_API_{13E}), and between (NOAPI_17E17M minus NOALL_17E17M, denote as ΔO_3_ARF_{17E}) and (NOAPI_13E17M minus NOALL_13E17M, denote as ΔO_3_ARF_{13E}), respectively. Detailed descriptions can be found in Fig. 1.

Simulation periods are integrated from 30 May to 30 June (denoted as summer) and 29 November to 31 December (denoted as winter) both in 2013 and 2017. To avoid potential deviations caused by long-term model integration, each simulation is re-initialized every eight days, with the first 40 hours as the model spin-up. The complete simulation includes five model cycles. Simulation results from the BASE_17E17M

case during summer and winter are used to evaluate the model performance. If not otherwise specified, the time in this paper is the local time, and the synergetic impacts of ARF and API are equal to the impact of ARI (i.e., ARI=ARF+API).

2.3 Observational data

Meteorological observations of temperature (T_2), relative humidity (RH_2), wind speed (WS_{10}) and wind direction (WD_{10}) provided by the NOAA's National Climatic Data Center (https://www.ncei.noaa.gov/) are used to validate the model meteorological performance. In this study, 353 meteorological stations are selected and the locations are shown as red dots in Fig. S1. Observed surface $PM_{2.5}$, O_3 and NO_2 concentrations in eastern China are obtained from the China National Environmental Monitoring Center, which can be downloaded from http://beijingair.sinaapp.com. To ensure the data quality, a single site with at least 500 actual observations during the simulated period are used for model evaluation. A total of 1296 sites, as shown in Fig. 2a, are obtained. Photolysis rates of nitrogen dioxide (NO_2) (J[NO_2]) measured at the Peking University site (39.99 °N, 116.31 °E) are also used to evaluate the model performance.

2.4 Integrated process rate analysis

Process analysis techniques, i.e., integrated process rate (IPR) analysis, can be used in grid-based Eulerian models (e.g., WRF-Chem) to obtain contributions of each physical/chemical process to variations in pollutant concentrations. Eulerian models utilize the numerical technique of operator splitting to solve continuity equations for each species into several simple ordinary differential equations or partial differential equations that only contain the influence of one or two processes (Gipson, 1999).

In order to quantitatively elucidate individual contributions of physical and chemical processes to O_3 concentration changes due to weakened ARI, the integrated process rate (IPR) methodology is applied in this study. IPR analysis is an advanced tool to evaluate the key process for O_3 concentration variation (Shu et al., 2016; Zhu et al., 2021; Yang et al., 2022). In this study, the IPR analysis tracks hourly (e.g., one time step) contribution to O_3 concentration variation from four main processes, including

vertical mixing (VMIX), net chemical production (CHEM), horizontal advection (ADVH), and vertical advection (ADVZ). VMIX is initiated by turbulent process and closely related to PBL development, which influences O_3 vertical gradients. CHEM represents the net O_3 chemical production (chemical production minus chemical consumption). ADVH and ADVZ represent transport by winds. We define ADV as the sum of ADVH and ADVZ.

3. Model Evaluation

Simulation results of BASE_17E17M are used to compare with the observations to evaluate the model performs before interpreting the impacts of aerosol-radiation interaction on surface-layer ozone concentration.

3.1 Evaluation for meteorology

Figure S2 shows the time series of observed and simulated T_2, RH_2, WS_{10}, and WD_{10} averaged over the 353 meteorological stations in China during summer and winter in 2017. Statistical performances of simulated meteorological parameters compared with ground-based observations are shown in Table 2. Simulations track well with observed T_2 with the correlation coefficient (R) of 0.99 and 0.92, but underestimate T_2 with the mean bias (MB) of -1.0 and -2.0 K in summer and winter, respectively. Simulated RH_2 agree reasonably well with observations with R of 0.97 and 0.87, and small normalized mean biases (NMB) are found in summer and winter with values of 3.2% and 3.5%, respectively. WS_{10} is slightly overpredicted with the MB of 1.6-2.1 m s^{-1}. The R and root-mean-square error (RMSE) of WS_{10} are 0.77-0.82 and 1.6-2.1 m s^{-1}, respectively. Large bias in wind speed can be partly caused by unresolved topographical features (Jimenez and Dudhia, 2012). The NMB of WD_{10} ranges from -3.9% to -2.6% and the R ranges from 0.40 to 0.69, respectively. As shown in Fig. S3, the predicted $J[NO_2]$ match well with the observations with R of 0.93-0.94 and NMB of 4.8%-12.3%. In general, the simulated meteorological variables fairly well agreement with the observations.

3.2 Evaluation for air pollutants

Figure 2 shows the spatial-temporal variations of observed and simulated near-surface $PM_{2.5}$, O_3 and NO_2 concentrations averaged over eastern China during summer and winter in 2017. As demonstrated in Figs. 2(a1) and (c1), WRF-Chem model reasonably well reproduces the spatial distribution of observed $PM_{2.5}$, with high values over large city cluster. The predicted O_3 concentrations can also reproduce the spatial variation of the observed concentrations (Figs. 2(a2) and (c2)). NO_2 is an important precursor of O_3 and aerosol, a good performance on NO_2 is necessary. From Figs. 2(a3) and (c3), the model can well reproduce the spatial distribution of observed NO_2. Although the distributions of simulated air pollutants are in good with the observations, biases still exist, which may be due to the uncertain in the emission inventories. Figures 2(b1-b3) and 2(d1-d3) show the temporal profiles of observed and simulated surface-layer air pollutants averaged over monitoring sites and the grid cell containing the monitor site in eastern China. The statistical metrics are also shown in Table 2. As shown in Figs. 2(b1) and (d1), the model tracks well with the diurnal variation of $PM_{2.5}$ over the eastern China, with R of 0.63 and 0.80, respectively. But the model slightly underestimates the concentrations of $PM_{2.5}$ with MB of -6.3 and -10.1 μg m^{-3}, respectively, in summer and winter. Simulated O_3 agree reasonably well with observations with R of 0.90 and 0.86, and small MB are found in summer and winter with values of -0.6 and 2.8 ppb, respectively. The model tracks the daily variation of observed NO_2 reasonably well, with R of 0.73 and 0.83. But the model slightly underestimates the NO_2 against measurements, with MB of -1.5 and -4.5 ppb, respectively, in summer and winter. In general, WRF-Chem model can well reproduce the features of observed meteorology and air pollutants over eastern China.

3.3 Evaluation for changes in air pollutants from 2013 to 2017

Figure 3 demonstrates the spatial distribution of changed summer (left) and winter (right) surface (a, b) $PM_{2.5}$ and (c, d) MDA8 O_3 from 2013 to 2017. As shown in Figs. 3(a) and 3(b), the observed concentrations of $PM_{2.5}$ in eastern China are significantly reduced both in summer (-16.2 μg m^{-3}) and winter (-56.0 μg m^{-3}), and these changes can be well captured by the model (-14.3 μg m^{-3} for summer and -49.8 μg m^{-3} for winter).

Therefore, the model can reproduce the observed decrease in $PM_{2.5}$ levels from 2013 to 2017. As shown in Figs. 3(c) and 3(d), the model reasonably well reproduces the seasonal patterns of changed surface MDA8 O_3 over the eastern China during summer and winter from 2013 to 2017. In summer, both the observations and simulations show the increased (decreased) MDA8 O_3 in YRD (PRD and SCB), while the model can not simulate the positive changes in MDA8 O_3 over BTH, and the potential reasons may be that this study did not consider the effect of changes in aerosol heterogeneous reactions. Li et al. (2019) found that the weakened uptake of HO_2 on aerosol surfaces was the main reason for the O_3 increase over BTH. In contrast to the changes in summer, observed MDA8 O_3 in winter generally increased over the eastern China, which can be well reproduced by the model.

4. Results and Discussion

4.1 Impacts of changed meteorology and anthropogenic emission on O_3

The strategy of clean air action decreased the anthropogenic emission of NO_x, but the changes in anthropogenic VOCs emissions were unobvious (Fig. S4), which might influence the O_3 formation sensitive regime and the O_3 concentration. Figure 4 shows the spatial distributions of changed summer and winter MDA8 O_3 concentrations from 2013 to 2017 due to changed anthropogenic emissions alone and changed meteorological conditions alone. As shown in Fig. 4(a), the concentration of summer MDA8 O_3 from 2013 to 2017 was increased in city clusters, but it was decreased in rural regions. This discrepancy might be explained by the ozone formation regimes in urban (typically VOCs-limited) and rural (typically NO_x-limited) areas during summer (Li et al., 2019; Wang et al., 2019). Contrary to the phenomenon in summer, decreased anthropogenic emissions lead to a uniform increase in winter MDA8 O_3 over the whole eastern China (Fig. 4(c)). These different spatial variation characteristics in summer and winter could be explained by the different ozone formation regimes in winter (VOCs-limited) and summer (NO_x-limited) (Fig. S5, Jin and Holloway, 2015). From Figs. 4(b) and (d), the impacts of changed meteorological conditions on MDA8 O_3 varied by regions, ranging from -24.9 (-14.0) to 17.0 (7.3) ppb in summer (winter). Focusing on

the four developed city clusters, compared with 2013, the meteorological conditions in the summer of 2017 promoted the generation of O_3 in the YRD region (Fig. 8(a3)), but suppressed the generation of O_3 in the BTH (Fig. 8(a2)), PRD (Fig. 8(a4)) and SCB (Fig. 8(a5)) regions. In PRD and SCB, the changes in MDA8 O_3 due to meteorology even have a greater impact than that by emission changes, which highlights the significant role of meteorology on summer O_3 variations.

4.2 Impacts of weakened aerosol-radiation interaction on O_3

Figures S6a (S7a) and S6b (S7b) present the spatial distribution of the impacts of ARF, API and ARI on surface MDA8 O_3 concentrations in summer (winter) under different anthropogenic emission conditions in year 2017 and year 2013, respectively. As shown in Fig. S6, summer MDA8 O_3 are significantly reduced over eastern China, ARF, API and ARI decrease the surface MDA8 O_3 concentrations by 0.23 (0.59) ppb, 1.09 (1.54) ppb and 1.32 (2.13) ppb under low (high) anthropogenic emission conditions in year 2017 (year 2013), respectively. The changes in MDA8 O_3 concentrations due to aerosol-radiation interaction under low emission condition are weaker than that under high emission condition. This is because the concentration of aerosols in year 2013 is higher than that in year 2017, and then its impact on meteorological conditions and J[NO_2] is greater (Fig. S8). As shown in Fig. S7a, ARF, API and ARI decrease the winter MDA8 O_3 concentrations by 0.38 ppb (-0.9%), 1.59 ppb (-4.1%) and 1.96 ppb (-5.1%) in year 2017, respectively. Compared to the impacts under relatively high anthropogenic emission conditions in year 2013, the reduction of surface MDA8 O_3 concentrations caused by ARF, API and ARI are also greater, with the values of 0.62 ppb (-1.6%), 1.98 ppb (-5.4%) and 2.59 ppb (-7.1%), respectively. Both API and ARF reduce O_3 concentrations, and the reduction in O_3 caused by API is greater than that caused by ARF both in summer and winter.

Further, the significant reduction in $PM_{2.5}$ due to clean air action (Fig. S9) will lead to an increase in O_3 concentrations as the weakened effects of aerosols on O_3. Therefore, this study further quantifies the effects of ΔO_3_ΔARF_EMI, ΔO_3_ΔAPI_EMI and ΔO_3_ΔARI_EMI (ΔO_3_ΔARI_EMI = ΔO_3_ΔARF_EMI + Δ

O_3_ΔAPI_EMI) on O_3 air quality. As shown in Figs. 5(a1-a3), the surface MDA8 O_3 in summer are increased over most of eastern China due to ΔO_3_ΔARF_EMI, ΔO_3_ΔAPI_EMI and ΔO_3_ΔARI_EMI. The largest increases in MDA8 O_3 concentrations due to ΔO_3_ΔARF_EMI and ΔO_3_ΔAPI_EMI are found in the developed four city clusters, with the increase larger than 4 ppb. Overall, ΔO_3_ΔARF_EMI, ΔO_3_ΔAPI_EMI and ΔO_3_ΔARI_EMI lead to the increase in surface MDA8 O_3 by 0.36 ppb, 0.45 ppb and 0.81 ppb averaged over eastern China during summer, respectively. As shown in Fig. 5(a4-a6), the ΔO_3_ΔARF_EMI, ΔO_3_ΔAPI_EMI and ΔO_3_ΔARI_EMI can also cause an increase in winter MDA8 O_3 concentrations by 0.24 ppb, 0.39 ppb and 0.63 ppb, respectively. In general, weakened aerosol-radiation interaction due to reduced anthropogenic emission from 2013 to 2017 can exacerbate ozone pollution both in summer and winter.

In order to explore the mechanism of the impacts of ΔO_3_ΔARI_EMI on MDA8 O_3, we resolve the changed O_3 into the contributions from chemical and physical processes. Figure 6 presents the accumulated changes in O_3 and each process contribution from 09:00 to 16:00 LST by the ΔO_3_ΔAPI_EMI, ΔO_3_ΔARF_EMI and ΔO_3_ΔARI_EMI during summer and winter. As shown in Fig 6, the enhanced chemical production is the dominant process leading to the increase in O_3 concentrations over eastern China and the four city clusters both in summer and winter. The leading factor of enhancement in O_3 over BTH are inconsistent with that over eastern China, and the enhancement of O_3 concentration in BTH is mainly due to ΔO_3_ΔARF_EMI. But the leading factor of enhancement in O_3 over SCB are consistent with that in eastern China, the enhancement of O_3 concentration is mainly due to ΔO_3_ΔAPI_EMI both in summer and winter. Moreover, the enhancement of O_3 concentration in BTH, YRD and PRD is mainly due to ΔO_3_ΔARF_EMI during winter, which is opposite to that of eastern China. The leading factors for the increase of O_3 concentration in different city clusters are different. The enhancement of O_3 concentration in most areas is caused by ΔO_3_ΔAPI_EMI, whereas the increase in O_3 concentration in BTH, YRD and PRD areas is dominated by ΔO_3_ΔARF_EMI in winter. In general, the weakened aerosol-radiation interaction caused by emission reduction would promote the chemical

production of O_3 and increase the O_3 concentrations over eastern China in summer and winter.

In order to explore the reason for the increase in O_3 chemical production, we further analyzed the variation of HO_x ($HO+HO_2$) concentration from 2013 to 2017. As the aerosol concentration decreases, its influence on solar radiation is weakened and photolysis is enhanced, leading to an increase in HO_x levels. It can be seen from Fig. S10 that the concentration of HO_x increases both in winter and summer. The increase in HO_x will promote the conversion of NO to NO_2, which will lead to the accumulation of O_3 concentration.

Figure 7 shows the changed summer and winter surface-layer MDA8 O_3 concentrations caused by anthropogenic emission reduction from 2013 to 2017 with (ΔO_3_EMI) and without (ΔO_3_NOARI) ARI, including the effects of weakened ARI on the effectiveness of emission reduction for O_3 air quality (ΔO_3_ΔARI_EMI, which is also equal to ΔO_3_EMI minus ΔO_3_NOARI). As shown in Figs. 7(a1) and 7(a4), the surface-layer MDA8 O_3 concentrations increased mainly in urban areas during summer and increased uniformly in winter due to anthropogenic emission reduction from 2013 to 2017 without the impact of ARI. When the effect of ARI is considered, the concentrations of MDA8 O_3 are increased more than that when ARI is not taken into account (Figs. 7(a2) and 7(a5)). The consequences of weakened ARI resulted from anthropogenic emission reduction on MDA8 O_3 concentrations are shown in Figs. 7(a3) and 7(a6). From Figs. 7(a3) and 7(a6) we can find that the concentrations of MDA8 O_3 are increased in both summer and winter over eastern China. Therefore, ΔO_3_ΔARI_EMI makes the superimposed impact on the effectiveness of anthropogenic emission reduction for the increased MDA8 O_3 concentrations from 2013 to 2017 over eastern China. However, during summer, the worsened O_3 air quality due to weakened ARI can only be found in scattered city clusters (e.g., BTH, YRD and PRD in Fig. 7(a3)). During winter, it will increase MDA8 O_3 concentrations over nearly the whole eastern China (Fig. 7(a6)).

We also average the observed MDA8 O_3 concentrations of monitoring sites in the urban areas and the simulation value for the grid cell containing the monitoring site to

further examine the impacts of changed meteorological conditions, anthropogenic emissions and ARI on O_3 levels in densely populated urban areas (Fig. 8). Given that most of the monitoring stations with 5 years of continuous observations are located in urban areas. Therefore, these monitoring stations and the grid cells containing the monitoring stations can be considered as urban areas in this study (Liu and Wang, 2020b). As shown in Figs. 8(a1) and 8(b1), the changes in observed MDA8 O_3 over urban areas in eastern China from 2013 to 2017 can be well captured by WRF-Chem both in summer and winter. In summer, changed meteorological conditions from 2013 to 2017 has little impact on the variations in MDA8 O_3 over the urban areas, while the contribution of emission reductions to increased MDA8 O_3 is significant. In winter, changed meteorological conditions is unfavorable for the increase in MDA8 O_3 from 2013 to 2017, indicating the worsened ozone pollution driven by the changed anthropogenic emission. What's more, the ΔO_3_ΔARI_EMI has significant effect on the increased MDA8 O_3 in summer from 2013 to 2017 with the value of +1.77 ppb (87.6%), but its impacts in winter are smaller, only +0.42 ppb (11.8%), which is consistent with the results in Li et al. (2021). The increased MDA8 O_3 concentration over urban areas in summer caused by O_3_ΔARI_EMI in this study is 1.77 ppb, which is compared to the value of 2.12 ppb increase caused by weakened aerosol heterogeneous reactions quantified by Liu and Wang (2020b). Meanwhile, the contributions of ΔO_3_ΔAPI_EMI and ΔO_3_ΔARF_EMI to the increase in O_3 concentration averaged over urban areas in eastern China are almost the same in summer (0.79 vs. 0.98) and winter (0.20 vs. 0.22). In general, we find that the enhancement of O_3 concentrations both in summer and winter is mainly caused by the factor of reduced anthropogenic emissions. Furthermore, the contributions of ΔO_3_ΔAPI_EMI and ΔO_3_ΔARF_EMI to the increases in O_3 concentrations from 2013 to 2017 over urban areas are almost the same during summer and winter.

4.3 Discussions

(1) The CBMZ gas-phase chemistry coupled with MOSAIC aerosol module

(CBMZ-MOSAIC for short) used in this study does not include secondary organic aerosol (SOA), then we applied three additional chemical mechanisms that consider SOA, namely, RADM2 gas-phase chemistry coupled with MADE/SORGAM aerosol module (RADM2-MADE/SORGAM for short), CBMZ gas-phase chemistry coupled with MADE/SORGAM aerosol module (CBMZ-MADE/SORGAM for short), and MOZART gas-phase chemistry coupled with MOSAIC aerosol module (MOZART-MOSAIC for short), to test the impact of ARI on O_3 with and without SOA for the scenario of BASE_17E17M.

Figures S11 shows the temporal variations of observed and simulated $PM_{2.5}$ and O_3 concentrations over eastern China for the three additional chemical mechanisms. Comparing with the observed $PM_{2.5}$ (O_3) concentrations, the MOZART-MOSAIC showed the best performance in December 2017, with the R of 0.73 (0.79) and NMB of -18.7% (-20.5%). Therefore, we further used this mechanism to simulate the air pollutant concentrations during the period of June 2017. As shown in Fig. S11 (a4, b4), the temporal variations of observed $PM_{2.5}$ (O_3) can be well captured by this mechanism with R of 0.56 (0.91) and NMB of -1.7% (-20.3%).

Finally, we investigated the effect of ARI on O_3 from the results of CBMZ-MOSAIC (this mechanism applied in this manuscript which does not include SOA) and MOZART-MOSAIC (this mechanism includes SOA and performs the best simulation results comparing with RADM2-MADE/SORGAM and CBMZ-MADE/SORGAM). As shown in Fig. S12, summer (winter) MDA8 O_3 is significantly reduced over eastern China, ARI reduces the surface MDA8 O_3 concentrations by 1.32 (1.96) ppb and 1.85 (1.60) ppb by CBMZ-MOSAIC and MOZART-MOSAIC, respectively. The O_3 reductions are of comparable magnitude in these two schemes. Therefore, we can conclude that although the CBMZ-MOSAIC applied in this manuscript does not take into account the formation of SOA and its associated effects, the aerosol radiative effects on O_3 concentrations not only in the pattern of spatial-temporal distribution but also in the order of magnitude are consistent with the results when the SOA simulation mechanism is considered.

As shown in Fig. S13, the mean SOA simulated by RADM2-MADE/SORGAM,

CBMZ-MADE/SORGAM, and MOZART-MOSAIC are 0.29, 0.45 and 0.94 μg m^{-3}, accounting for 3.4%, 3.8%, and 4.4% of $PM_{2.5}$ concentrations in winter 2017, respectively. From Fig. S14, the mean SOA simulated from MOZART-MOSAIC is 0.90 μg m^{-3}, account for 9.1% of $PM_{2.5}$ in summer 2017. Model simulated SOA concentrations are generally underestimated in most current chemical transport models (Zhang et al., 2015; Zhao et al., 2015). The low SOA concentrations simulated by the model can be explained by low emissions of biogenic and anthropogenic VOCs (key precursors of SOA), but a thorough investigation of this underestimation is outside the scope of this manuscript and it will be discussed in our future work.

(2) The impacts of aerosol heterogeneous reactions (HET) on O_3 have not been considered in this manuscript due to the uncertainty and inconsistency of the heterogeneous uptake shown in previous observation and simulation studies (Liu and Wang., 2020b; Tan et al., 2020; Shao et al., 2021). Liu and Wang. (2020b) found that the rapid decrease of $PM_{2.5}$ was the primary contributor for the summer O_3 increase through weakening the heterogeneous uptake of hydroperoxy radical (HO_2). However, Tan et al. (2020) launched a field campaign in NCP and proposed a contradicting opinion about the importance of the impact of HET on O_3. Shao et al. (2021) summarized that different heterogeneous uptake on the aerosol surface applied in the model simulation (e.g., 0.20 *vs.* 0.08) would cause significant deviations in simulated ozone concentrations (e.g., O_3 increased by 6% *vs.* O_3 increased by 2.5%). Previous laboratory studies indicate that the dependence of the uptake coefficient on aerosol composition and RH means that a single assumed value for heterogeneous uptake used in numerical simulations can lead to large uncertainties (Lakey et al., 2015; Taketani et al., 2009; Zou et al., 2019). Therefore, the uncertainty in the heterogeneous uptake value used in the numerical simulation will finally amplify the deviation in model results. Meanwhile, our manuscript devoted to quantifying the effects of ARI on O_3, rather than the impacts of heterogeneous reactions on O_3. The absence of heterogeneous chemistry on aerosol surface may result in underestimation of the effect of aerosol on O_3, which will be considered in our future work.

(3) There may be an interaction between API and ARF. However, in this study we

discuss the role of API and ARF separately, which may ignore the effects of interactions between API and ARF on O_3. This may affect our results, and we will discuss their interaction in our future studies.

5 Conclusions

In this study, the impact of weakened aerosol-radiation interaction (ARI) due to decreased anthropogenic emissions on surface O_3 (ΔO_3_ΔARI_EMI) over eastern China is mainly analyzed by using an online-coupled regional chemistry transport model WRF-Chem. Simulation results generally reproduce the spatiotemporal characteristics of observations with correlation coefficients of 0.63-0.90 for pollutant concentrations and 0.40-0.99 for meteorological parameters, respectively.

Sensitivity experiments show that the changes in MDA8 O_3 from 2013 to 2017 over eastern China vary spatially and seasonally, and the decreased anthropogenic emission plays a more prominent role for the MDA8 O_3 increase than the impact of changed meteorological conditions both in summer and winter. Furthermore, the decreased $PM_{2.5}$ concentrations due to reduced anthropogenic emissions can result in a weaker impact of ARI on O_3 concentrations, which finally pose a superimposed effect on the worsened O_3 air quality. For urban areas over eastern China, ΔO_3_ΔARI_EMI has a significant effect on the increase of MDA8 O_3 in summer with the value of +1.77 ppb, accounting for 87.6% of the increased value caused by decreased anthropogenic emissions, but the impacts in winter are smaller (+0.42 ppb), accounting for 11.8% of the increased value caused by decreased anthropogenic emissions. For the whole regions over eastern China, the enhancement of MDA8 O_3 by ΔO_3_ΔARI_EMI is +0.81 (+0.63) ppb, with ΔO_3_ΔAPI_EMI and ΔO_3_ΔARF_EMI contributing for 55.6% (61.9%) and 44.4% (38.1%) in summer (winter), respectively. Process analysis shows that the enhanced O_3 chemical production is the dominant process for the increased O_3 concentrations caused by ΔO_3_ΔARI_EMI both in summer and winter.

Generally, since China's clean air action from 2013, the decreased $PM_{2.5}$ concentrations due to reduced anthropogenic emissions can worsen O_3 air quality by the weakened interactions between aerosol and radiation, which is a new and an

important implication for understanding the causes driving the increases in O_3 level over eastern China. Therefore, our results highlight that more carefully designed multi-pollutants coordinated emissions control strategies are needed to reduce the concentrations of $PM_{2.5}$ and O_3 simultaneously.

Data availability

The observed hourly surface concentrations of air pollutants are derived from the China National Environmental Monitoring Center (http://www.cnemc.cn). The observed surface meteorological data are obtained from NOAA's National Climatic Data Center (https://gis.ncdc.noaa.gov/maps/ncei/cdo/hourly). The photolysis rates of nitrogen dioxide in Beijing are provided by Xin Li (li_xin@pku.edu.cn). The simulation results can be accessed by contacting Lei Chen (chenlei@nuist.edu.cn) and Hong Liao (hongliao@nuist.edu.cn).

Author contributions

HY, LC, and HL conceived the study and designed the experiments. HY and LC performed the simulations and carried out the data analysis. JZ, WW, and XL provided useful comments on the paper. HY prepared the paper with contributions from all co-authors.

Competing interests

The authors declare that they have no competing interests.

Acknowledgements

This work is supported by National Natural Science Foundation of China (Grant 42305121, 42007195, 42293320), National Key R&D Program of China (Grant 2019YFA0606804, 2022YFE0136100), and Natural Science Foundation of Jiangsu Province (Grant BK20220031), Guizhou Provincial Science and Technology Projects of China (CXTD [2022]001, GCC [2023]026), and Open fund by Jiangsu Key Laboratory of Atmospheric Environment Monitoring and Pollution Control (KHK 2211).

Reference

Atkinson, R.: Atmospheric chemistry of VOCs and NOx, Atmos Environ., 34, 2063–2101, https://doi.org/10.1016/S1352-2310(99)00460-4, 2000.

Chen, F. and Dudhia, J.: Coupling an Advanced Land Surface – Hydrology Model with the Penn State – NCAR MM5 Modeling System. Part I: Model Implementation and Sensitivity, Mon. Weather Rev., 129(4), 569–585, 2001.

Dang, R. and Liao, H.: Radiative Forcing and Health Impact of Aerosols and Ozone in China as the Consequence of Clean Air Actions over 2012–2017, Geophys. Res. Lett., 46, 12511–12519, https://doi.org/10.1029/2019GL084605, 2019.

Foken, T.: 50 years of the Monin-Obukhov similarity theory, Bound.-Layer Meteor., 119, 431–437, 2006.

Gipson, G. L.: Science algorithms of the EPA Models-3 community multiscale air quality (CMAQ) modeling system: Chapter 16, process analysis, edited by: Byun, D. W. and Ching, J. K. S., Reported No. EPA/600/R-99/030, U.S. Environmental Protection Agency, Office of Research and Development, Washington, D.C., 1999.

Grell G A.: Prognostic evaluation of assumptions used by cumulus parameterizations, Monthly Weather Review., 121, 764–787, 1993.

Grell, G. A., Peckham, S. E., Schmitz, R., Mckeen, S. A., Frost, G., Skamarock, K., and Eder, B.: Fully coupled “online” chemistry within the WRF model, Atmos. Environ., 39, 6957–6975, 2005.

Guenther, A., Karl, T., Harley, P., Wiedinmyer, C., Palmer, P. I., and Geron, C.: Estimates of global terrestrial isoprene emissions using MEGAN (Model of Emissions of Gases and Aerosols from Nature), Atmos. Chem. Phys., 6, 3181–3210, doi:10.5194/acp-6-3181-2006, 2006.

Hong, C., Zhang, Q., Zhang, Y., Davis, S. J., Zhang, X., Tong, D., Guan, D., Liu, Z., and He, K.: Weakening aerosol direct radiative effects mitigate climate penalty on Chinese air quality, Nat. Clim. Change, 10, 845–850, https://doi.org/10.1038/s41558-020-0840-y, 2020.

Hong, S.-Y., Noh, Y., and Dudhia, J.: A New Vertical Diffusion Package with an

Explicit Treatment of Entrainment Processes, Mon. Weather Rev., 134, 2318–2341, 2006.

Iacono, M. J., Delamere, J. S., Mlawer, E. J., Shephard, M. W., Clough, S. A., and Collins, W. D.: Radiative forcing by long-lived greenhouse gases: Calculations with the AER radiative transfer models, J. Geophys. Res., 113, D13103, doi:10.1029/2008JD009944, 2008.

Jimenez, P. A. and Dudhia, J.: Improving the representation of resolved and unresolved topographic effects on surface wind in the WRF model, J. Appl. Meteorol. Clim., 51, 300–316, 2012.

Jin, X. and Holloway, T.: Spatial and temporal variability of ozone sensitivity over China observed from the Ozone Monitoring Instrument, J. Geophys. Res.-Atmos., 120, 7229–7246, https://doi.org/10.1002/2015JD023250, 2015.

Lakey, P. S. J., George, I. J., Whalley, L. K., Baeza-Romero, M. T., and Heard, D. E.: Measurements of the HO_2 Uptake Coefficients onto Single Component Organic Aerosols, Environmental Science & Technology, 49, 4878-4885, 10.1021/acs.est.5b00948, 2015.

Lelieveld, J., Evans, J. S., Fnais, M., Giannadaki, D., and Pozzer, A.: The contribution of outdoor air pollution sources to premature mortality on a global scale, Nature, 525, 367–371, https://doi.org/10.1038/nature15371, 2015.

Li, K., Jacob, D. J., Liao, H., Qiu, Y. L., Shen, L., Zhai, S. X., Bates, K. H., Sulprizio, M. P., Song, S. J., Lu, X., Zhang, Q., Zheng, B., Zhang, Y. L., Zhang, J. Q., Lee, H. C., and Kuk, K. S.: Ozone pollution in the North China Plain spreading into the late-winter haze season, 118, P. Natl. Acad. Sci. USA, https://doi.org/10.1073/pnas.2015797118, 2021.

Li, K., Jacob, D. J., Liao, H., Shen, L., Zhang, Q., and Bates, K. H.: Anthropogenic Drivers of 2013–2017 Trends in Summer Surface Ozone in China, P. Natl. Acad. Sci. USA, 116, 422–427, https://doi.org/10.1073/pnas.1812168116, 2019.

Li, K., Jacob, D. J., Shen, L., Lu, X., De Smedt, I., and Liao, H.: Increases in surface ozone pollution in China from 2013 to 2019: anthropogenic and meteorological

influences, Atmos. Chem. Phys., 20, 11423–11433, https://doi.org/10.5194/acp-20-11423-2020, 2020.

Liao, H., Yung, Y. L., and Seinfeld, J. H.: Effects of aerosols on tropospheric photolysis rates in clear and cloudy atmospheres, J. Geophys. Res., 104, 23697–23707, 1999.

Lin, Y.-L., Farley, R. D., and Orville, H. D.: Bulk parameterization of the snow field in a cloud model, J. Clim. Appl. Meteorol., 22, 1065–1092, 1983.

Liu, Y. and Wang, T.: Worsening urban ozone pollution in China from 2013 to 2017 – Part 1: The complex and varying roles of meteorology, Atmos. Chem. Phys., 20, 6305–6321, https://doi.org/10.5194/acp-20-6305-2020, 2020a.

Liu, Y. and Wang, T.: Worsening urban ozone pollution in China from 2013 to 2017 – Part 2: The effects of emission changes and implications for multi-pollutant control, Atmos. Chem. Phys., 20, 6323–6337, https://doi.org/10.5194/acp-20-6323-2020, 2020b.

Lou, S., Liao, H., and Zhu, B.: Impacts of aerosols on surface-layer ozone concentrations in China through heterogeneous reactions and changes in photolysis rates, Atmos. Environ., 85, 123–138, 2014.

Lu, X., Hong, J. Y., Zhang, L., Cooper, O. R., Schultz, M. G., Xu, X. B., Wang, T., Gao, M., Zhao, Y. H., and Zhang, Y. H.: Severe surface ozone pollution in China: A global perspective, Environ. Sci. Tech. Lett., 5, 487–494, https://doi.org/10.1021/acs.estlett.8b00366, 2018.

Mills, G., Sharps, K., Simpson, D., Pleijel, H., Broberg, M., Uddling, J., Jaramillo, F., Davies, W. J., Dentener, F., Van den Berg, M., Agrawal, M., Agrawal, S. B., Ainsworth, E. A., Buker, P., Emberson, L., Feng, Z., Harmens, H., Hayes, F., Kobayashi, K., Paoletti, E., and Van Dingenen, R.: Ozone pollution will compromise efforts to increase global wheat production, Glob. Change Biol., 24, 3560–3574, https://doi.org/10.1111/gcb.14157, 2018.

Seinfeld, J. H. and Pandis, S. N.: Atmospheric Chemistry and Physics: from Air Pollution to Climate Change, second ed., John Wiley and Sons, 2006.

Shao, M., Wang, W. J., Yuan, B., Parrish, D. D., Li, X., Lu, K. D., Wu, L. L., Wang, X. M., Mo, Z. W., Yang, S. X., Peng, Y. W., Kuang, Y., Chen, W. H., Hu, M., Zeng,

L. M., Su, H., Cheng, Y. F., Zheng, J. Y., Zhang, Y. H.: Quantifying the role of $PM_{2.5}$ dropping in variations of ground-level ozone: Inter-comparison between Beijing and Los Angeles, Sci. Total Environ., https://doi.org/10.1016/j.scitotenv.2021.147712, 2021.

Shu, L., Wang, T., Han, H., Xie, M., Chen, P., Li, M., and Wu, H.: Summertime ozone pollution in the Yangtze River Delta of eastern China during 2013–2017: Synoptic impacts and source apportionment, Environ. Pollut., 257, 113631, https://doi.org/10.1016/j.envpol.2019.113631, 2020.

Shu, L., Xie, M., Wang, T., Gao, D., Chen, P., Han, Y., Li, S., Zhuang, B., and Li, M.: Integrated studies of a regional ozone pollution synthetically affected by subtropical high and typhoon system in the Yangtze River Delta region, China, Atmos. Chem. Phys., 16, 15801–15819, https://doi.org/10.5194/acp-16-15801- 2016, 2016.

Skamarock, W., Klemp, J. B., Dudhia, J., Gill, D. O., Barker, D. M., Duda, M., Huang, X. Y., Wang,W., and Powers, J. G.: A description of the advanced research WRF version 3, NCAR technical note NCAR/TN/u2013475, 2008.

Taketani, F., Kanaya, Y., and Akimoto, H.: Heterogeneous loss of HO_2 by KCl, synthetic sea salt, and natural seawater aerosol particles, Atmospheric Environment, 43, 1660-1665, 2009.

Tan Z, Hofzumahaus A, Lu K, Brown SS, Holland F, Huey LG, et al. No Evidence for a Significant Impact of Heterogeneous Chemistry on Radical Concentrations in the North China Plain in Summer 2014. Environ. Sci. Technolc. 54, 5973-5979, 2020.

Wang, J., Allen, D. J., Pickering, K. E., Li, Z., and He, H.: Impact of aerosol direct effect on East Asian air quality during the EAST-AIRE campaign, J. Geophys. Res.-Atmos., 121, https://doi.org/10.13016/M27W0S, 2016.

Wang, N., Lyu, X., Deng, X., Huang, X., Jiang, F., and Ding, A.: Aggravating O3 pollution due to NOx emission control in eastern China, Sci. Total Environ., 677, 732–744, 2019.

Wild, O., Zhu, X., and Prather, M. J.: Fast-J: Accurate simulation of in- and below-cloud photolysis in tropospheric chemical models, J. Atmos. Chem., 37, 245–282, doi:10.1023/A:1006415919030, 2000.

Yang, H., Chen, L., Liao, H., Zhu, J., Wang, W., and Li, X.: Impacts of aerosol–photolysis interaction and aerosol–radiation feedback on surface-layer ozone in North China during multi-pollutant air pollution episodes, Atmos. Chem. Phys., 22, 4101–4116, https://doi.org/10.5194/acp-22-4101-2022, 2022.

Yue, X., Unger, N., Harper, K., Xia, X., Liao, H., Zhu, T., Xiao, J., Feng, Z., and Li, J.: Ozone and haze pollution weakens net primary productivity in China, Atmos. Chem. Phys., 17, 6073–6089, https://doi.org/10.5194/acp-17-6073-2017, 2017.

Zaveri, R. A. and Peters, L. K.: A new lumped structure photochemical mechanism for large-scale applications, J. Geophys. Res., 104, D23, 30387–30415, https://doi.org/10.1029/1999JD900876, 1999.

Zaveri, R. A., Easter, R. C., Fast, J. D., and Peters, L. K.: Model for simulating aerosol interactions and chemistry (MOSAIC), J. Geophys. Res., 113, D13204, https://doi.org/10.1029/2007JD008782, 2008.

Zhai, S., Jacob, D. J., Wang, X., Shen, L., Li, K., Zhang, Y., Gui, K., Zhao, T., and Liao, H.: Fine particulate matter (PM2.5) trends in China, 2013–2018: separating contributions from anthropogenic emissions and meteorology, Atmos. Chem. Phys., 19, 11031–11041, https://doi.org/10.5194/acp-19-11031-2019, 2019.

Zhang, B., Wang, Y., and Hao, J.: Simulating aerosol–radiation–cloud feedbacks on meteorology and air quality over eastern China under severe haze conditions in winter, Atmos. Chem. Phys., 15, 2387–2404, https://doi.org/10.5194/acp-15-2387-2015, 2015.

Zhang, Q., Zheng, Y., Tong, D., Shao, M., Wang, S., Zhang, Y., Xu, X., Wang, J., He, H., Liu, W., Ding, Y., Lei, Y., Li, J., Wang, Z., Zhang, X., Wang, Y., Cheng, J., Liu, Y., Shi, Q., Yan, L., Geng, G., Hong, C., Li, M., Liu, F., Zheng, B., Cao, J., Ding, A., Gao, J., Fu, Q., Huo, J., Liu, B., Liu, Z., Yang, F., He, K., and Hao, J.: Drivers of Improved PM2.5 Air Quality in China from 2013 to 2017, P. Natl. Acad. Sci. USA, 116, 24463–24469, https://doi.org/10.1073/pnas.1907956116, 2019.

Zhao, B., Wang, S., Donahue, N. M., Chuang, W., Ruiz, L. H., Ng, N. L., Wang, Y., and Hao, J.: Evaluation of One-Dimensional and Two-Dimensional Volatility Basis Sets in Simulating the Aging of Secondary Organic Aerosol with Smog-Chamber

Experiments, Environ. Sci. Technol., 49, 2245–2254, doi:10.1021/es5048914, 2015.

Zheng, B., Tong, D., Li, M., Liu, F., Hong, C., Geng, G., Li, H., Li, X., Peng, L., Qi, J., Yan, L., Zhang, Y., Zhao, H., Zheng, Y., He, K., and Zhang, Q.: Trends in China's anthropogenic emissions since 2010 as the consequence of clean air actions, Atmos. Chem. Phys., 18, 14095–14111, https://doi.org/10.5194/acp-18-14095-2018, 2018.

Zhu, J., Chen, L., Liao, H., Yang, H., Yang, Y., and Yue, X.: Enhanced PM2.5 Decreases and O3 Increases in China During COVID-19 Lockdown by Aerosol-Radiation Feedback, Geophys. Res. Lett., 48, https://doi.org/10.1029/2020GL090260, 2021.

Zou Q, Song H, Tang M, Lu K. Measurements of HO_2 uptake coefficient on aqueous $(NH_4)_2SO_4$ aerosol using aerosol flow tube with LIF system. Chinese Chemical Letters. 30, 2236-2240, 2019.

Table 1. Descriptions of model sensitivity experiments.

Cases	Anthropogenic emission	Meteorological field	API[a]	ARF[a]
BASE_17E17M	2017	2017	On	On
BASE_13E13M	2013	2013	On	On
NOAPI_17E17M	2017	2017	Off	On
NOALL_17E17M	2017	2017	Off	Off
BASE_13E17M	2013	2017	On	On
NOAPI_13E17M	2013	2017	Off	On
NOALL_13E17M	2013	2017	Off	Off

[a]API means aerosol-photolysis interaction, ARF means aerosol-radiation feedback.

Table 2. Statistical parameters of the simulated 2 m temperature (T_2, k), 2 m relative humidity (RH_2, %), 10 m wind speed (WS_{10}, m s^{-1}), 10 m wind direction (WD_{10}, °), photolysis rate of NO_2 ($J[NO_2]$, 10^{-3} s^{-1}), $PM_{2.5}$ (μg m^{-3}), O_3 (ppb), and NO_2 (ppb) against observations during summer and winter in 2017. There are 1296 air pollutant monitoring stations and 353 meteorological stations.

	Summer						Winter					
Variable	**O**[a]	**M**[a]	**R**[b]	**MB**[c]	**NMB**[d] **(%)**	**RMSE**[e]	**O**[a]	**M**[a]	**R**[b]	**MB**[c]	**NMB**[d] **(%)**	**RMSE**[e]
T_2	295.3	294.2	0.99	-1.0	-3.2	1.0	275.0	272.8	0.92	-2.0	-74.1	2.5
RH_2	68.1	71.0	0.97	2.2	3.2	3.6	58.1	60.6	0.87	2.1	3.5	6.5
WS_{10}	2.6	4.2	0.77	1.6	61.6	1.6	2.6	4.7	0.82	2.1	83.2	2.1
WD_{10}	175.7	170.9	0.40	-4.6	-2.6	16.9	192.6	184.6	0.69	-7.5	-3.9	17.4
$J[NO_2]$	2.6	2.7	0.93	0.1	4.8	1.2	1.0	1.2	0.94	0.1	12.3	0.6
$PM_{2.5}$	31.0	24.8	0.63	-6.3	-20.2	8.3	69.0	58.9	0.80	-10.1	-14.6	15.6
O_3	39.7	38.9	0.90	-0.6	-1.6	6.9	17.7	20.5	0.86	2.8	15.7	5.0
NO_2	12.7	11.2	0.73	-1.5	-12.0	4.5	23.3	18.7	0.83	-4.5	-19.4	5.6

[a]***O*** and ***M*** are the averages for observed and simulated results, respectively. $O = \frac{1}{n} \times \sum_{i=1}^{n} O_i$, $M = \frac{1}{n} \times \sum_{i=1}^{n} M_i$.

[b]***R*** is the correlation coefficient between observations and model results. $R = \frac{\sum_{i=1}^{n} |(O_i - O) \times (M_i - M)|}{\sqrt{\sum_{i=1}^{n} (O_i - O)^2 + \sum_{i=1}^{n} (M_i - M)^2}}$.

[c]***MB*** is the mean bias between observations and model results. $MB = \frac{1}{n} \times \sum_{i=1}^{n} (M_i - O_i)$.

[d]***NMB*** is the normalized mean bias between observations and model results. $NMB = \frac{1}{n} \times \sum_{i=1}^{n} \frac{M_i - O_i}{O_i} \times 100\%$.

[e]***RMSE*** is the root-mean-square error of observations and model results. $RMSE = \sqrt{\frac{1}{n} \times \sum_{i=1}^{n} (M_i - O_i)^2}$.

In the above O_i and M_i are the hourly observed and simulated data, respectively, and n is the total number of hours.

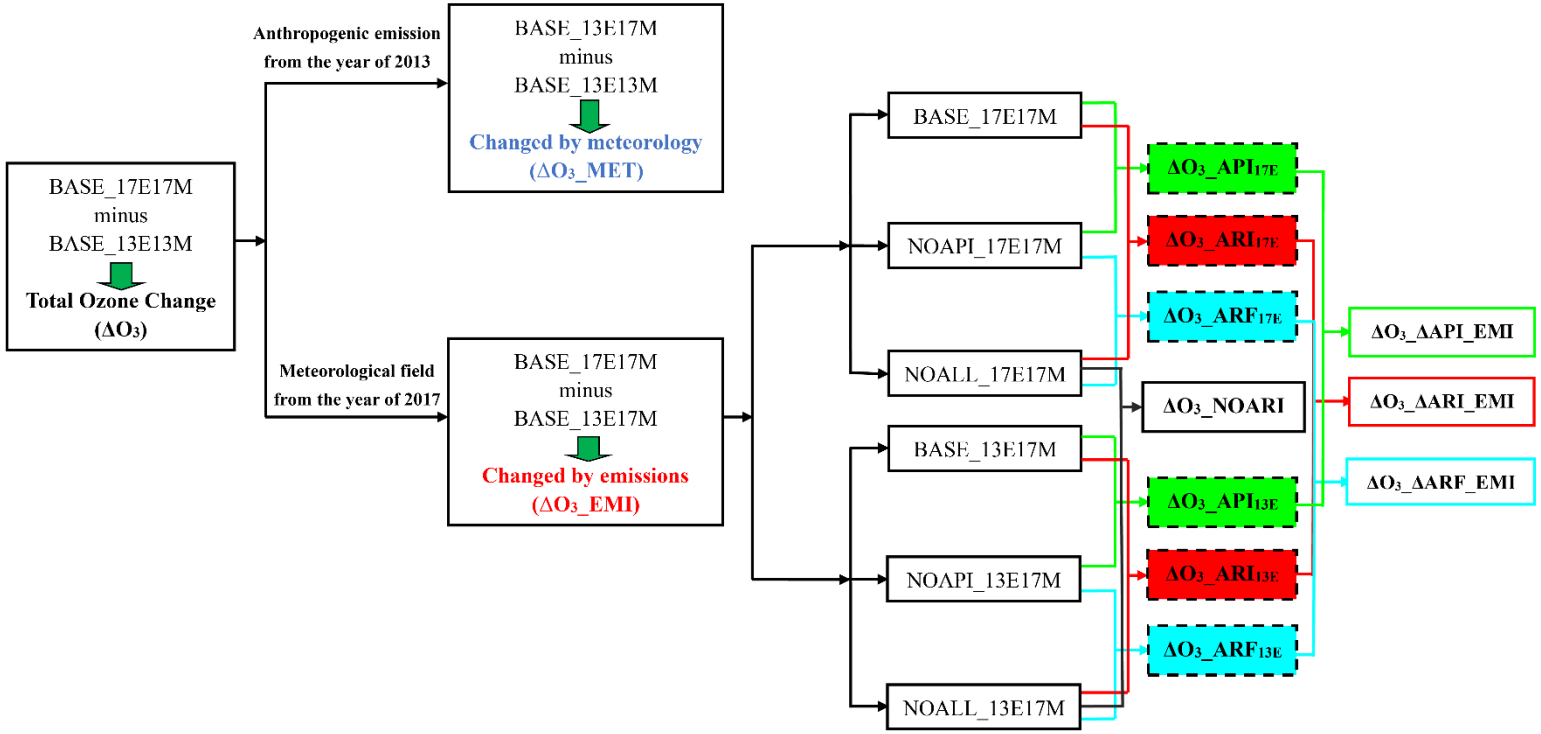

Figure 1. Schematic overview of numerical experiments. 17E17M (13E13M) means meteorological fields and anthropogenic emissions are from the year of 2017 (2013). 13E17M means anthropogenic emissions are from the year of 2013 but meteorological fields are at year 2017. ΔO_3_MET, ΔO_3_EMI and ΔO_3 mean the impacts of changed meteorological conditions, changed anthropogenic emissions and their combined effects on O_3, respectively. ΔO_3_$API_{17E(13E)}$, ΔO_3_$ARF_{17E(13E)}$ and ΔO_3_$ARI_{17E(13E)}$ mean the impacts of aerosol-photolysis interaction, aerosol-radiation feedback and aerosol-radiation interaction on O_3 under different emission conditions, respectively. ΔO_3_NOARI means the changed O_3 concentration by reduced anthropogenic emissions without considering aerosol-radiation interaction. ΔO_3_ΔAPI_EMI, ΔO_3_ΔARF_EMI and ΔO_3_ΔARI_EMI represent the impacts of weakened aerosol-photolysis interaction, aerosol-radiation feedback and aerosol-radiation interaction due to decreased anthropogenic emission on O_3 concentration, respectively.

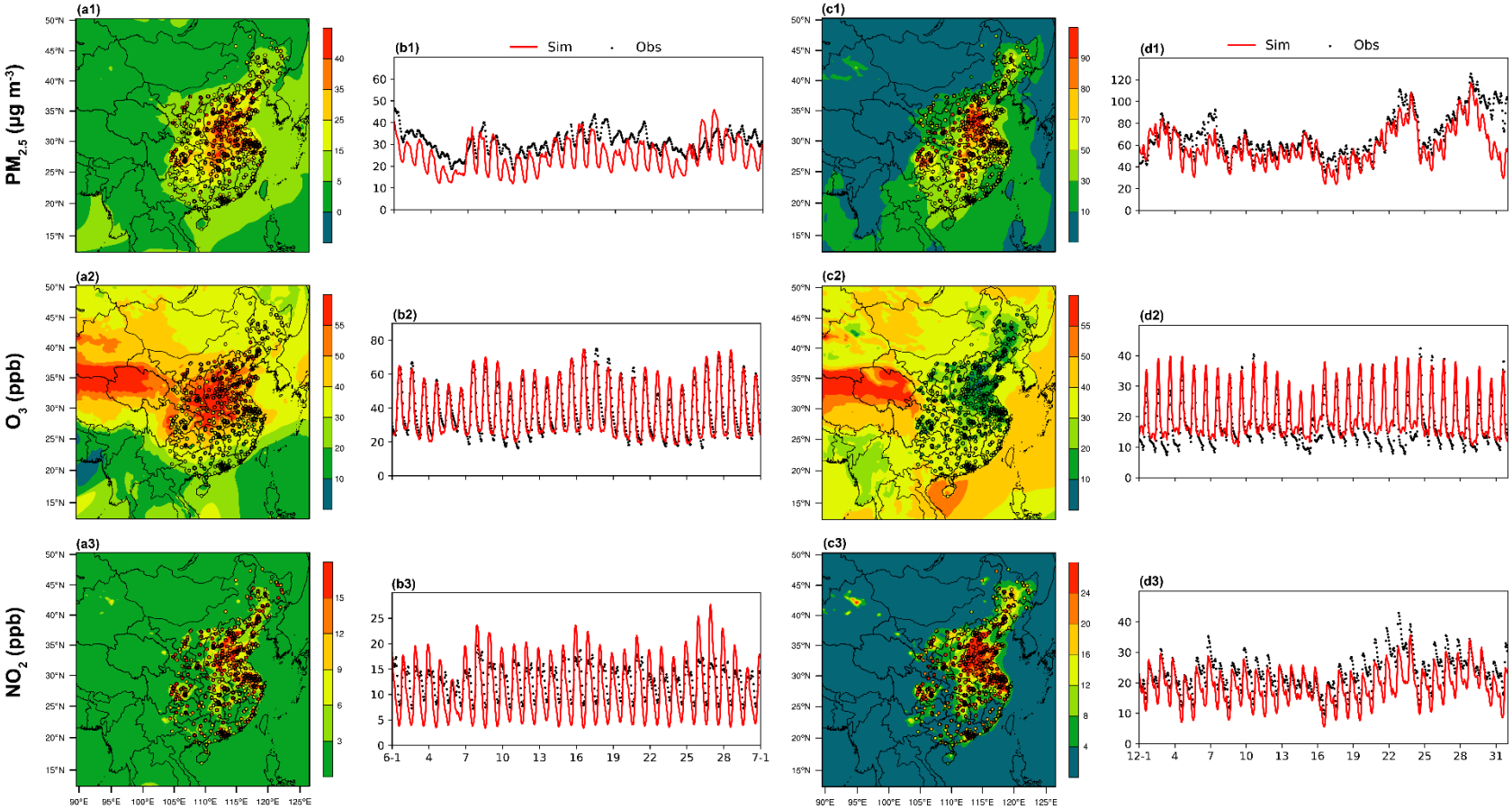

Figure 2. Spatial distributions of observed (circle) and simulated (shade) $PM_{2.5}$, O_3 and NO_2 concentrations averaged over (**a1-a3**) summer and (**c1-c3**) winter in 2017. Time series of observed (black dots) and simulated (red lines) hourly $PM_{2.5}$, O_3 and NO_2 concentrations averaged over the whole observation sites in eastern China during (**b1-b3**) summer and (**d1-d3**) winter in 2017.

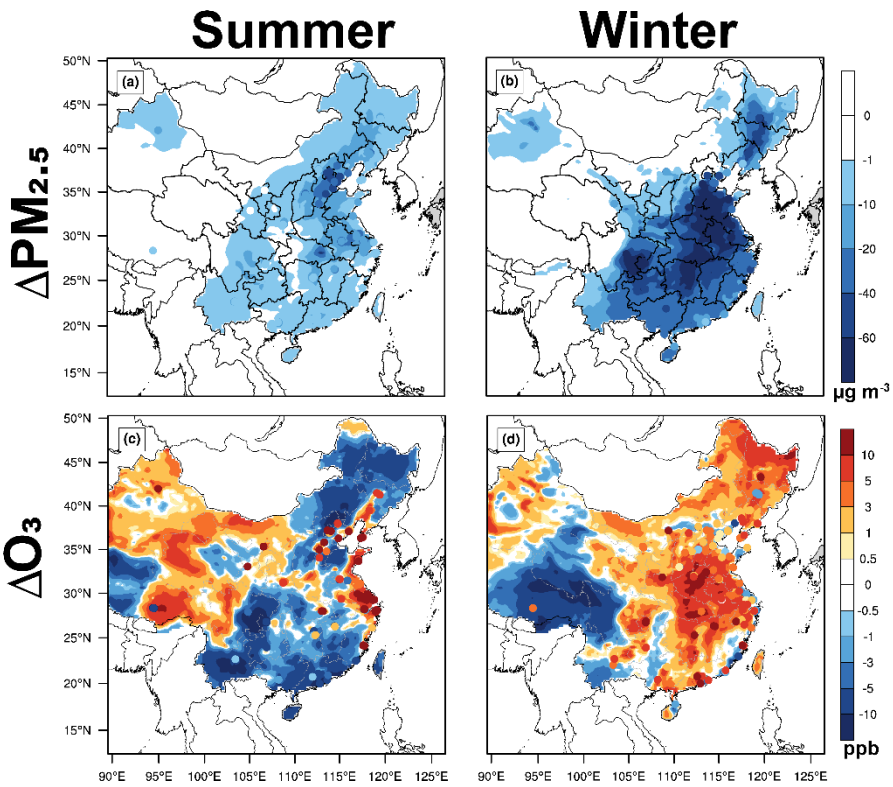

Figure 3. Spatial distribution of changed summer (left) and winter (right) surface **(a, b)** $PM_{2.5}$ and **(c, d)** MDA8 O_3 from 2013 to 2017. Observed changes in surface $PM_{2.5}$ MDA8 O_3 are also marked with colored circles.

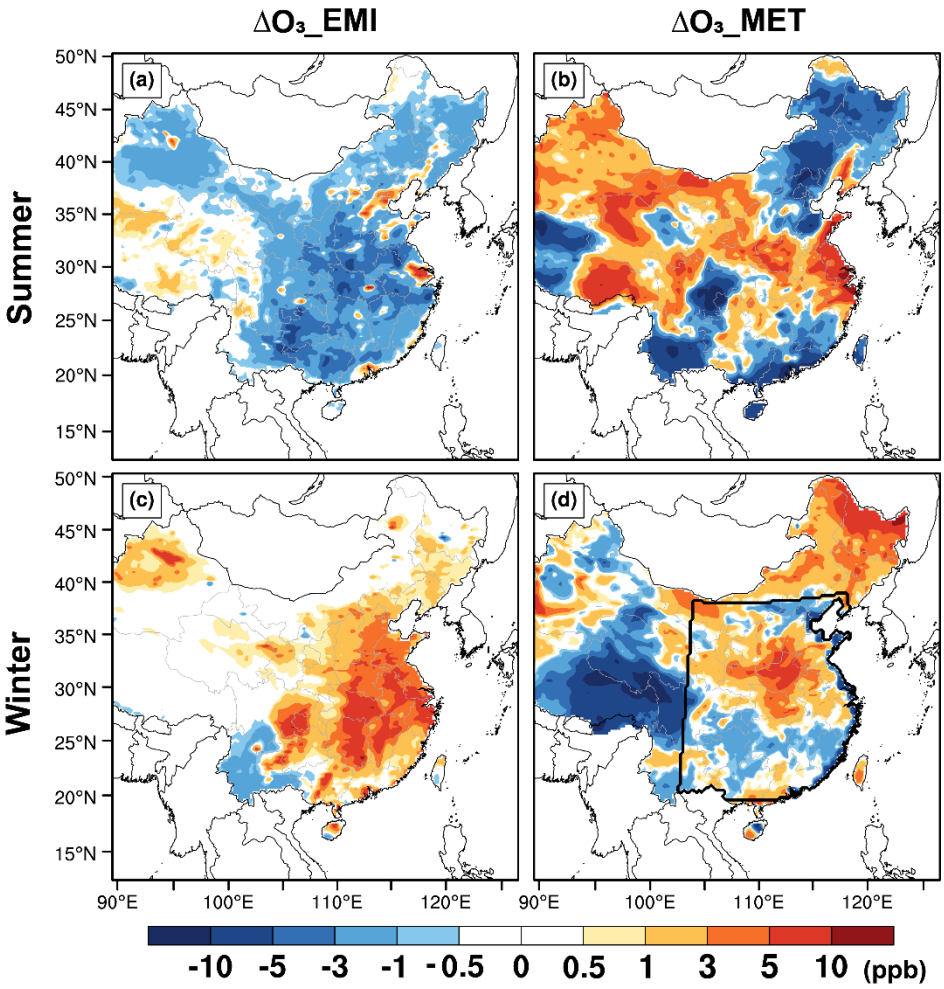

Figure 4. Spatial distribution of changed summer (upper) and winter (bottom) surface-layer MDA8 O_3 from 2013 to 2017 due to **(a, c)** changed anthropogenic emissions alone and **(b, d)** changed meteorological fields alone. The enclosed black line in **(d)** represents eastern China.

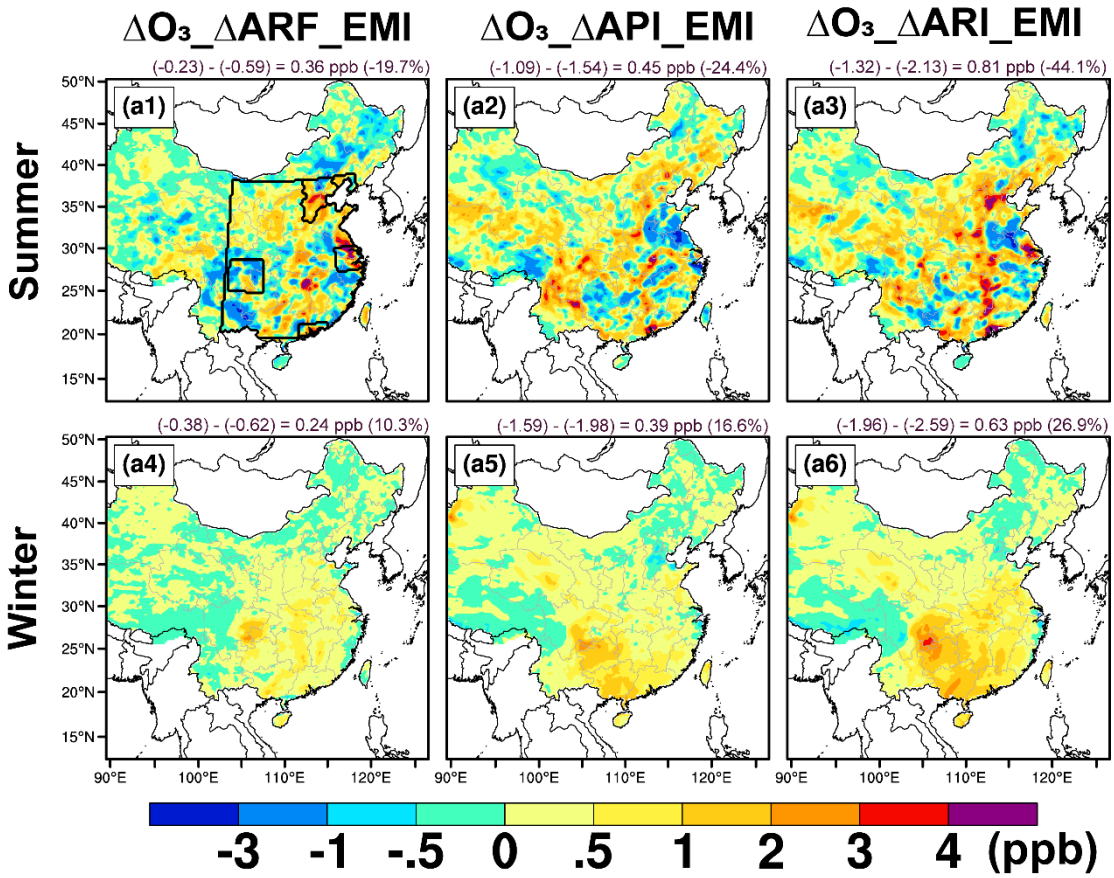

Figure 5. Impacts of ΔO_3_ΔARF_EMI, ΔO_3_ΔAPI_EMI, and ΔO_3_ΔARI_EMI on summer (upper) and winter (bottom) surface-layer MDA8 O_3 concentrations. The enclosed black line in **(a1)** represents eastern China and the four developed city clusters. The mean changes over eastern China are also shown at the top of each panel. Detailed information about ΔO_3_ΔARF_EMI, ΔO_3_ΔAPI_EMI, and ΔO_3_ΔARI_EMI can be found in Figure 1.

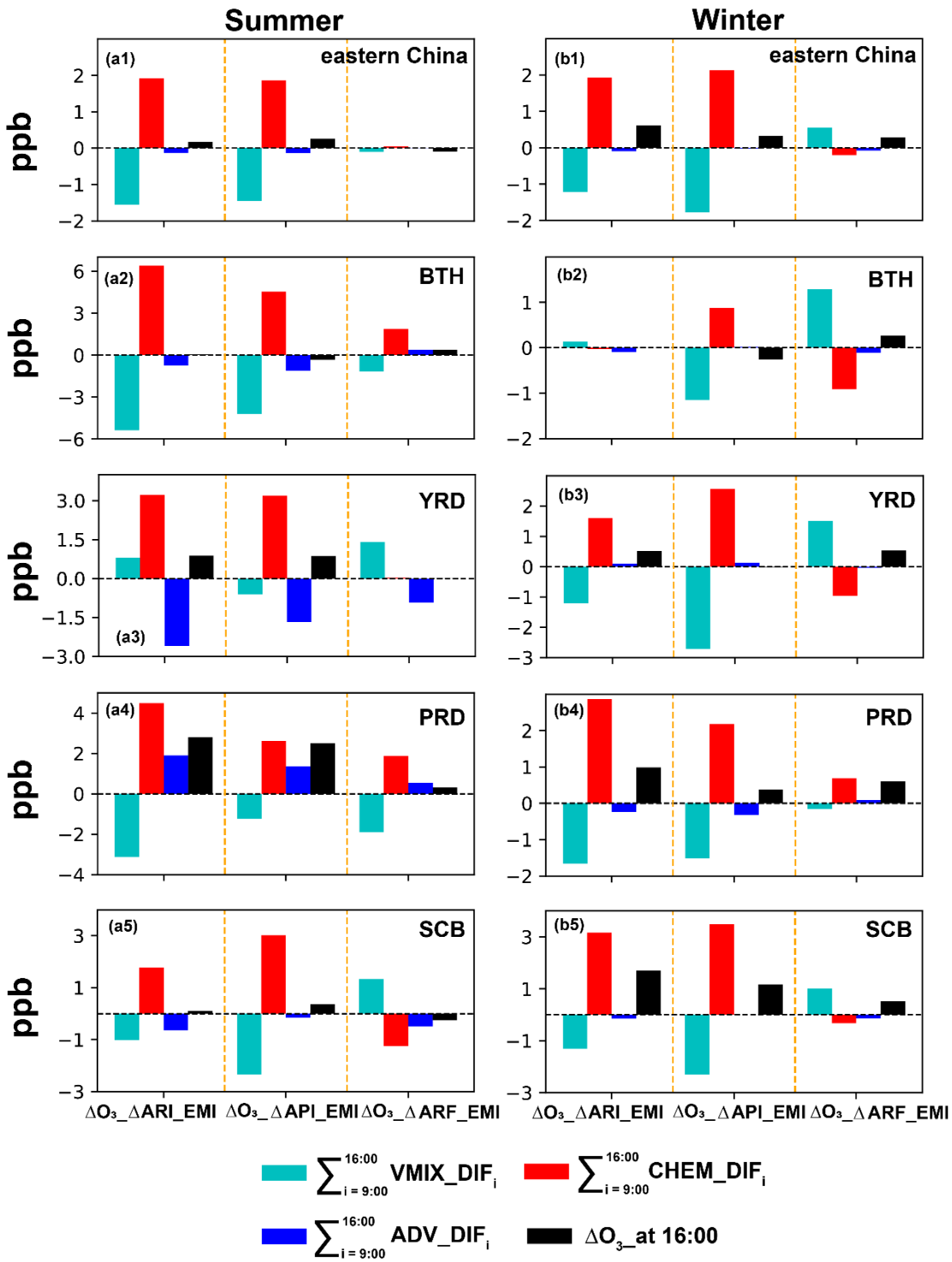

Figure 6. Accumulated changes in each process from 09:00 to 16:00 LST and the changed O_3 concentrations due to ΔO_3_ΔARI_EMI in summer (left column) and winter (right column). The regions of eastern China, Beijing-Tianjin-Hebei (BTH), Yangtze River Delta (YRD), Pearl River Delta (PRD) and Sichuan Basin (SCB) are indicated on the upper right side of each panel.

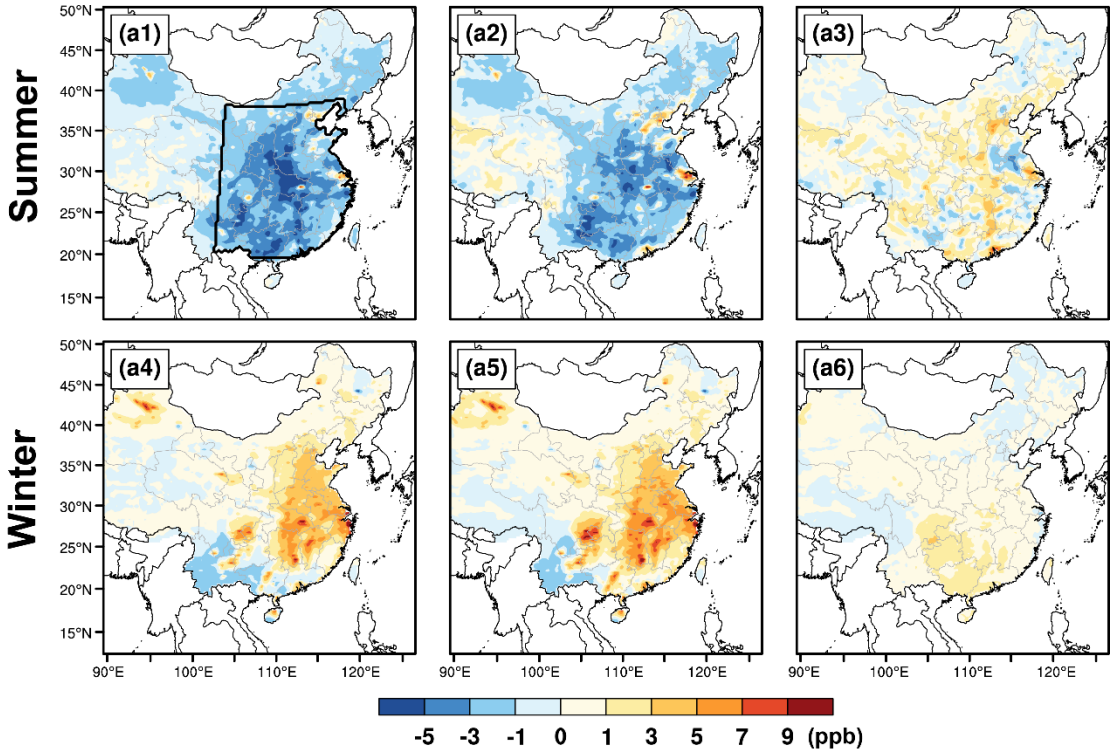

Figure 7. Spatial distribution of changed summer (upper) and winter (bottom) surface-layer MDA8 O_3 concentrations from sensitivity simulations. **(a1, a4)** Effects of anthropogenic emission reduction on MDA8 O_3 without ARI. **(a2, a5)** Effects of anthropogenic emission reduction on MDA8 O_3 with ARI. **(a3, a6)** Effects of weakened ARI on the effectiveness of emission reduction for O_3 air quality.

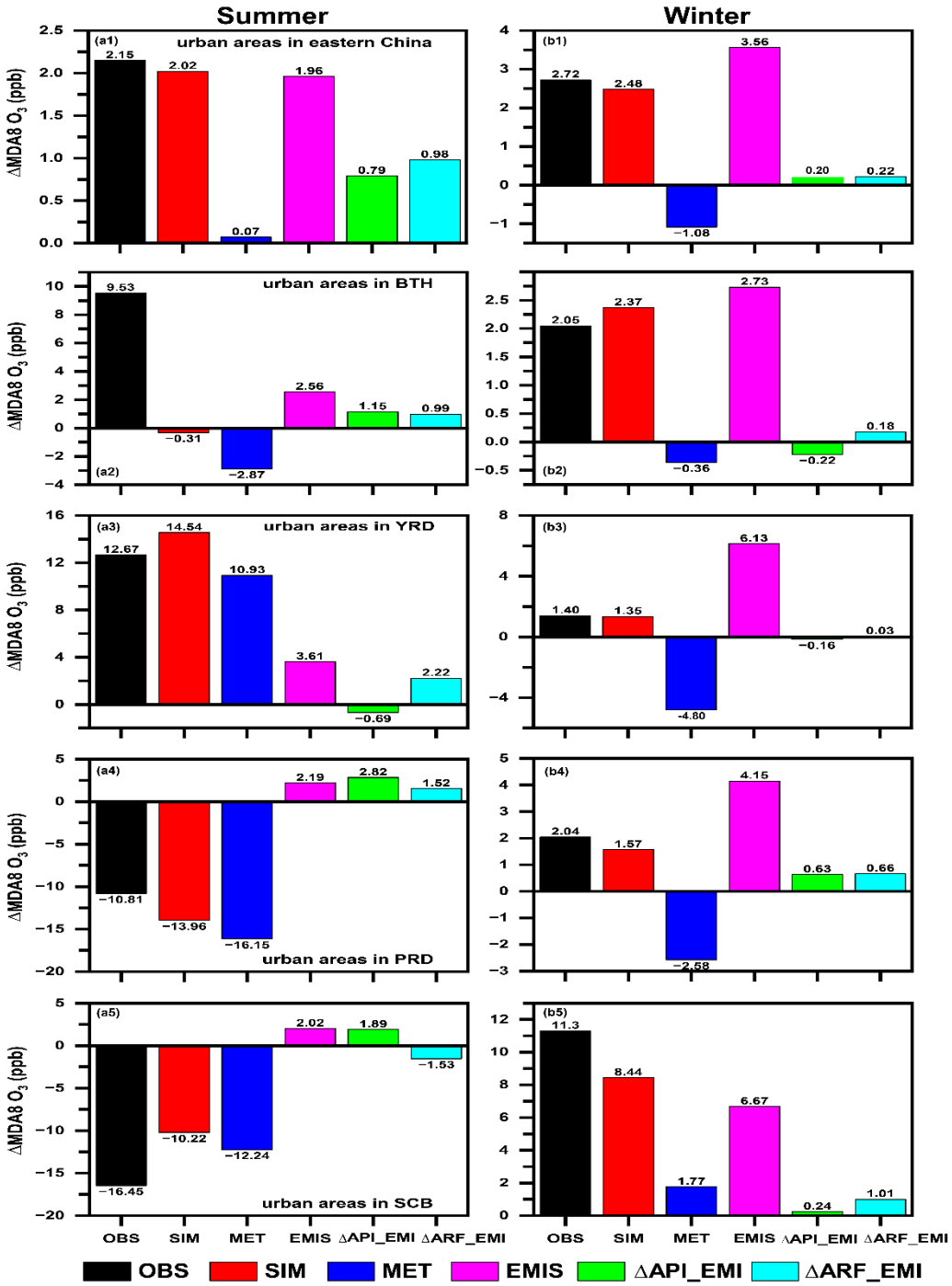

Figure 8. The observed (OBS, black bars) and simulated (SIM, red bars) changes in (left) summer and (right) winter surface-layer MDA8 O_3 from 2013 to 2017. Contributions of changed meteorological conditions alone (MET, blue bars), changed anthropogenic emissions alone (EMI, purple bars), changed aerosol-photolysis interaction alone (ΔAPI_EMI, green bars), and changed aerosol-radiation feedback alone (ΔARF_EMI, cyan bars) are also shown. Observations are calculated from the monitoring sites in the analyzed region, while the corresponding gridded simulations are averaged for SIM. **(a1-b1)**, **(a2-b2)**, **(a3-b3)**, **(a4-b4)** and **(a5-b5)** represent the urban areas in eastern China, Beijing-Tianjin-Hebei (BTH), Yangtze River Delta (YRD), Pearl River Delta (PRD), and Sichuan Basin (SCB), respectively.